Tube-based Robust Model Predictive Control for Tracking Control of Autonomous Articulated Vehicles

Dasol Jeong, Seibum B. Choi, *Member, IEEE,*

***Abstract*—Articulated vehicles play a critical role in the transportation industry, but the rise in truck-related accidents necessitates effective solutions. Autonomous driving presents a promising approach to enhancing safety. Among autonomous technologies, this paper presents a framework for an autonomous vehicle tracking control algorithm utilizing tube-based robust model predictive control (RMPC). The primary objective is to achieve precise path tracking while ensuring performance, safety, and robustness even with modeling errors. The framework adopts a lumped dynamics model for articulated vehicles, which reduces computational complexity while preserving linearity. Specific constraints of articulated vehicles are integrated to guarantee stability, safety, and adherence to actuator limits. The tube-based RMPC technique reliably satisfies constraints under worst-case scenarios, thereby addressing robustness against modeling errors. The proposed algorithm employs tube-based RMPC to ensure the safety and robustness of autonomous articulated vehicles. In the design of the tracking controller, error tube analysis between the actual plant and the prediction model plays a vital role. An error tube analysis method and framework are introduced through simulation. Performance evaluations of the proposed algorithm and previous tracking controllers are conducted through comparative simulations. Previous algorithms exhibited tracking errors exceeding 50 cm, posing potential safety risks. In contrast, the proposed algorithm demonstrates tracking errors of less than 50 cm. Furthermore, the proposed algorithm exhibits notable stability. The results demonstrate that the proposed algorithm enables accurate and safe tracking of complex autonomous articulated vehicles.**

***Index Terms*—Autonomous articulated vehicles, Autonomous driving, Tracking control, Robust tube-based model predictive control, Robustness.**

I. Introduction

ARTICULATED vehicles are essential in the transportation industry due to the advantage of having a hefty load capacity. However, the escalating number of trucks on the roads has resulted in a surge of property damage and human casualties caused by truck accidents [1]. Articulated vehicles are particularly susceptible to rollover accidents due to their higher center of gravity than other vehicles [2]. Moreover, simultaneously controlling the first and second units of articulated vehicles presents a significant challenge, making it difficult to prevent accidents. Consequently, the characteristics of trucks, including articulated vehicles, have induced frequent traffic accidents and human casualties [3].

Dasol Jeong is Senior Research Engineer, Hyundai Motor Company, 150 HyundaiYeonguso-ro, Namyang-eup, Hwaseong-si, Gyeonggi-do, 18280, Republic of Korea (jds5513@hyundai.com)

Seibum B. Choi is Professor at the School of Mechanical, Department of Mechanical Engineering, at the Korea Advanced Institute of Science and Technology (KAIST), 291 Daehak-ro, Yuseong-gu, Daejeon 305-338, Republic of Korea (e-mail: sbchoi@kaist.ac.kr).

TABLE I
Requirements of tracking controllers for autonomous articulated vehicles.

Requirements	Details
Performance	Vehicle width: $2.5\,m$, Lane width: $3.5 \sim 4\,m$
Stability	Roll-over, jackknife, trailer swing/oscillation
Robustness & Safety	Obstacle avoidance constraints

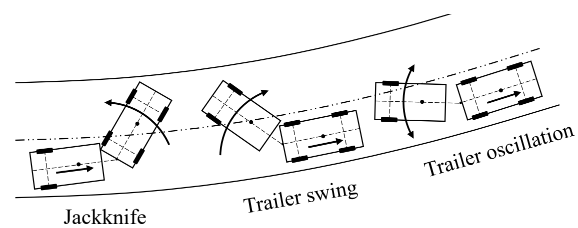

Fig. 1. Instability situations of articulated vehicles.

The advent of autonomous driving has drawn attention to a strategy with significant potential for mitigating the risk of truck accidents [4]. The development goals of autonomous driving for cars and trucks differ. Self-driving cars aim to provide both vehicle safety and driving convenience, albeit at a perceived high cost. In contrast, autonomous trucks offer distinct advantages in vehicle safety and cost reduction compared to passenger cars [5]. With the integration of autonomous capabilities, labor costs and transportation time associated with trucks can be minimized.

Autonomous driving encompasses various features, including adaptive cruise control [6], lane-keeping assist system [7], lane change functionality, and obstacle avoidance [8], [9]. Among the numerous autonomous driving technologies available, tracking control technology directly influences the vehicle's behavior. Hence, implementing safe autonomous articulated vehicles necessitates precise control [10].

The desired characteristics of the tracking controller for articulated vehicles are outlined in Table I. The target plant, the articulated vehicle, exhibits a significantly wider width than the passenger cars. Consequently, precise control is imperative to avert lane encroachment and collisions with obstacles. Moreover, inaccurate control leads to unstable behavior, as shown in Fig. 1. An advanced control method is indispensable to prevent jackknifing, trailer swing, and trailer oscillation [11]. Additionally, the controller must exhibit robustness against hard constraints, such as collision avoidance, which must be unconditionally satisfied. Hence, the tracking controller for articulated vehicles must prioritize performance, safety, and robustness.

Previous studies have mainly focused on two types of tracking control algorithms. The first type encompasses geometric controllers and classical control approaches. Among these, the pure-pursuit [12] and Stanley [13] algorithms are widely recognized as classical geometric tracking controllers [14]. The pure-pursuit algorithm involves projecting the vehicle's moving point onto a preplanned path, facilitating tracking of the desired trajectory from the current position. On the other hand, the Stanley algorithm utilizes nonlinear control principles to determine the steering angle based on lateral and angular errors, enabling effective tracking of a predetermined path. These algorithms commonly use in general driving scenarios where the vehicle follows a global path [15].

However, classical geometric tracking controllers exhibit limitations in severe driving conditions, such as obstacle avoidance, that necessitate precise tracking control. These limitations stem from factors such as the lack of consideration of vehicle dynamics, including tire models. Moreover, constraints cannot be considered, and this limitation may compromise vehicle safety. Consequently, geometric controllers are suitable for tracking global paths but inappropriate for all driving conditions, including severe driving.

The second tracking controller design approach utilizes model predictive control (MPC). MPC has garnered considerable attention in recent studies on obstacle avoidance for autonomous vehicles [16]. The most important thing is that MPC can effectively satisfy states and input constraints by fully considering vehicle dynamics [17]. It makes the MPC advantageous over other algorithms in ensuring vehicle safety. Furthermore, a cost function enables precise parameter tuning, which balances tracking control performance and control input. In conclusion, MPC offers notable advantages in tracking control performance, exhibiting stability and safety in global and local path tracking while delivering commendable tracking performance [18].

However, one crucial challenge must be addressed to utilize MPC for controller design effectively. This challenge pertains to ensuring robustness against modeling errors [19]. MPC relies on prediction models to predict future behavior and optimize control inputs. However, discrepancies inevitably exist between the actual plant and the prediction model, leading to modeling errors. These errors can violate original constraints imposed on the system's states. Such a scenario significantly impacts the stability and safety of the system, potentially leading to collision incidents when collision avoidance constraints are breached. Therefore, ensuring robustness against modeling errors becomes paramount to ensure the stability and safety of the system.

Previous studies have proposed robust MPC (RMPC) to ensure robustness, including tube-based RMPC [20], min-max RMPC [21], and stochastic RMPC [22]. Among these, tube-based RMPC stands out as it guarantees the satisfaction of the original constraints even under the worst conditions [23]. However, it adopts a conservative approach, which may limit system performance. For the collision-avoidance system of an autonomous vehicle, it is imperative to satisfy tracking error constraints, even if it means employing a conservative control strategy. Therefore, this study proposes a tracking controller for an autonomous articulated vehicle by leveraging the tube-based RMPC technique [24].

This study presents a novel framework for an autonomous vehicle tracking control algorithm utilizing a tube-based RMPC. The MPC framework comprises key components: cost function, prediction model, constraints, and constraint tightening. A combination of tracking error and control input-associated comfort is employed regarding the cost function. For the prediction model, several models are available, depending on the control objective. In previous studies, various models including lumped lateral dynamics [25], roll dynamics for preventing rollover [26], lateral dynamics for all-wheel steering vehicles [27], and nonlinear models [28] have been proposed. Among these models, the lumped lateral dynamics model has advantageous as it reduces the articulated vehicle to four states while maintaining linearity [25]. Consequently, this model significantly reduces computational complexity during RMPC construction compared to nonlinear models. This study develops a tracking controller based on this model. Constraints are incorporated to ensure stability, safety, and adherence to the actuator limits of the ego vehicle. Notably, constraints specifically considering the characteristics of articulated vehicles are introduced. To ensure robustness, a tube-based RMPC technique is adopted. Techniques such as error tube analysis and constraint tightening are introduced to handle modeling errors effectively. This robust approach ensures the safety and stability of autonomous articulated vehicles.

This study has two significant contributions. Firstly, we analyze the modeling error and maximal error between the prediction model and the actual plant to ensure robustness. The proposed analysis process can be used as a reference for ensuring autonomous articulated vehicles' robustness. Secondly, a comprehensive framework for an autonomous vehicle tracking controller is proposed. The prediction model and constraints utilized in the algorithm are universally applicable, enhancing the practicality and versatility of the proposed approach.

The rest of the paper is organized as follows. Section II introduces the prediction model for tracking control of autonomous articulated vehicles. In Section III, we propose a tracking control algorithm based on the tube-based RMPC approach. The proposed algorithm is designed to ensure performance, stability, and robustness. Section IV analyzes modeling errors and maximal error tubes between the actual plant and the prediction model. The performance validation results of the simulations are provided in Section V. Section VI presents the conclusion and future work.

II. Prediction model for autonomous articulated vehicles

A. Lumped lateral dynamics for articulated vehicles

In this study, we modeled autonomous articulated vehicles using the lumped lateral dynamics model [25]. The specifications, model parameters, and states of the vehicles are

TABLE II
SPECIFICATIONS OF THE ARTICULATED BUS USED IN THE EXPERIMENT.

Symbol	Parameter	Value
m_1	Total mass of first unit	$11180\,kg$
m_2	Total mass of second unit	$10130\,kg$
I_1	Yaw inertia of first unit	$60193\,kgm^2$
I_2	Yaw inertia of second unit	$54540\,kgm^2$
l_{f1}	Distance between 1^{st} axle to CG_1	$4.6260\,m$
l_{r1}	Distance between 2^{nd} axle to CG_1	$3.0840\,m$
P_1	Distance between 2^{nd} axle to hitch	$1.123\,m$
l_{f2}	Distance between hitch to CG_2	$3.8712\,m$
l_{r2}	Distance between 3^{rd} axle to CG_2	$2.5808\,m$
C_1	Cornering stiffness of the 1^{st} axle	$\sim 4.0E05\,N/rad$
C_2	Cornering stiffness of the 2^{nd} axle	$\sim 5.9E05\,N/rad$
C_3	Cornering stiffness of the 3^{rd} axle	$\sim 5.3E05\,N/rad$

TABLE III
STATES OF THE ARTICULATED VEHICLE.

Symbol	Parameter	Unit
δ	Front wheel steering angle	rad
β_i	Sideslip angle of the i^{th} unit	rad
r_i	Yaw rate of the i^{th}unit	rad/s
α	Articulated angle	rad
v_{yi}	Lateral velocity of the i^{th} unit	m/s
a_{yi}	Lateral acceleration of the i^{th} unit	m/s^2
F_{yi}	Lateral force of the i^{th} axle	N
F_{yh}	Lateral force of hitch	N

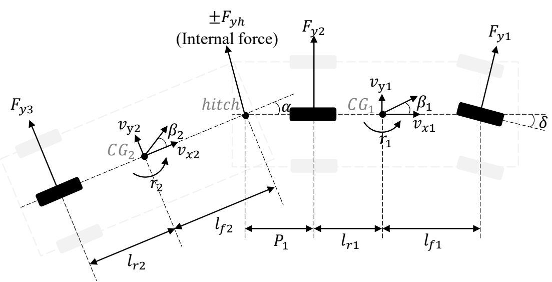

Fig. 2. The bicycle model of articulated vehicles.

presented in Tables II and III [25]. The specification and model parameters are based on the real-world articulated bus, as shown in Fig. 6.

The articulated vehicles were modeled based on a bicycle model, as shown in Fig. 2. The force and torque equilibrium equations for the center of gravity of the front and rear units are formulated as follows:

$$\begin{aligned} m_1 a_{y1} &= F_{yh} + F_{y1} + F_{y2} \\ m_2 a_{y2} &= -F_{yh} + F_{y3} \\ I_1 \dot{r}_1 &= -(P_1 + l_{r1})F_{yh} + l_{f1}F_{y1} - l_{r1}F_{y2} \\ I_2 \dot{r}_2 &= -l_{f2}F_{yh} - l_{r2}F_{y3} \end{aligned} \tag{1}$$

The kinematic constraints governing lateral acceleration and articulated angle are expressed as follows:

$$\begin{aligned} a_{y1} &= r_1 v_{x1} + \dot{\beta}_1 v_{x1} \\ a_{y2} &= r_2 v_{x2} + \dot{\beta}_2 v_{x2} \\ \dot{\alpha} &= r_2 - r_1 \end{aligned} \tag{2}$$

Maintaining linearity in the model brings computational advantages. Consequently, the lateral tire forces are represented using a linear tire model, as given by equation (3).

$$\begin{aligned} F_{y1} &= -C_1\alpha_1 = -C_1\left(\beta_1 + \frac{l_{f1}}{v_{x1}}r_1 - \delta\right) \\ F_{y2} &= -C_2\alpha_2 = -C_2\left(\beta_1 - \frac{l_{r1}}{v_{x1}}r_1\right) \\ F_{y3} &= -C_3\alpha_3 = -C_3\left(\beta_2 - \frac{l_{r2}}{v_{x2}}r_2\right) \end{aligned} \tag{3}$$

Lumped lateral dynamics model reduces the model states using several physical constraints as follows [25]:

- Lateral velocity at the hitch point

$$\beta_2 = \beta_1 - \alpha - \frac{(l_{r1} + P_1)r_1 + l_{f2}r_2}{v_x} \tag{4}$$

- Lateral force at the hitch point

$$\begin{aligned} F_{yh} &= -\frac{l_{r2}}{l_{f2} + l_{r2}} m_2 v_x \\ &\times \left(\dot{\beta}_1 + r_1 - \frac{l_{r1} + P_1}{v_x}\dot{r}_1 + \frac{I_2 - l_{f2}l_{r2}m_2}{l_{r2}m_2 v_x}\dot{r}_2\right) \end{aligned} \tag{5}$$

Finally, the articulated vehicles were modeled through a combination of the bicycle model, linear tire model, and the imposed physical constraints, resulting in the following lumped lateral dynamics model:

$$\begin{gathered} \text{Let, } \mathbf{x_m} = \begin{bmatrix} v_{y1} & r_1 & r_2 & \alpha \end{bmatrix}^T, \mathbf{u_m} = \delta, \\ \dot{\mathbf{x}}_\mathbf{m} = \mathbf{A}\mathbf{x_m} + \mathbf{B}\mathbf{u_m}, \\ \text{where } \mathbf{A} = \mathbf{T_0^{-1}}\mathbf{A_0}, \mathbf{B} = \mathbf{T_0^{-1}}\mathbf{B_0}, \end{gathered}$$

$$\begin{gathered} \mathbf{T_0} = \begin{bmatrix} t_{11} & t_{12} & t_{13} & 0 \\ t_{21} & t_{22} & t_{23} & 0 \\ t_{31} & t_{32} & t_{33} & 0 \\ 0 & 0 & 0 & 1 \end{bmatrix}, \\ \mathbf{A_0} = \begin{bmatrix} a_{11} & a_{12} & 0 & 0 \\ a_{21} & a_{22} & 0 & 0 \\ a_{31} & a_{32} & a_{33} & a_{34} \\ 0 & -1 & 1 & 0 \end{bmatrix}, \mathbf{B_0} = \begin{bmatrix} b_1 \\ b_1 \\ 0 \\ 0 \end{bmatrix}, \\ t_{11} = 1 + \frac{l_{r2}}{L_2}\frac{m_2}{m_1}, t_{12} = -\frac{l_{r2}(P_1 + l_{r2})}{L_2}\frac{m_2}{m_1}, \\ t_{13} = \frac{1}{L_2}\frac{I_2 - l_{f2}l_{r2}m_2}{m_1}, t_{21} = -\frac{(P_1 + l_{r1})l_{r2}}{L_2}\frac{m_2}{I_1}, \\ t_{22} = 1 + \frac{(P_1 + l_{r1})^2 l_{r2}}{L_2}\frac{m_2}{I_1}, t_{23} = -\frac{P_1 + l_{r1}}{L_2}\frac{I_2 - l_{f2}l_{r2}m_2}{I_1}, \\ t_{31} = -\frac{l_{f2}l_{r2}}{L_2}\frac{m_2}{I_1}, t_{32} = 1 + \frac{(P_1 + l_{r1})^2}{L_2}\frac{m_2}{I_1}, \\ t_{33} = \frac{l_{r2}}{L_2}\frac{I_2 + l_{f2}^2 m_2}{I_2} \\ a_{11} = -\frac{C_1 + C_2}{m_1 v_x}, a_{12} = \frac{-C_1 l_{f1} + C_2 l_{r1}}{m_1 v_x} - \left(1 + \frac{l_{r2}}{L_2}\frac{m_2}{m_1}\right) v_x, \\ a_{21} = \frac{-C_1 l_{f1} + C_2 l_{r1}}{I_1 v_x}, a_{22} = \frac{-C_1 l_{f1}^2 - C_2 l_{r1}^2}{I_1 v_x} + \frac{(P_1 + l_{r1})l_{r2}}{L_2}\frac{m_2 v_x}{I_1}, \\ a_{31} = \frac{C_3 l_{r2}}{I_2 v_x}, a_{32} = \frac{-C_1 l_{r2}(P_1 + l_{r1})}{I_2 v_x} + \frac{l_{f2}l_{r2}}{L_2}\frac{m_2 v_x}{I_2}, \\ a_{33} = -\frac{C_3 l_{r2} L_2}{I_2 v_x}, a_{34} = -\frac{C_3 l_{r2}}{I_2} \\ b_1 = \frac{C_1}{m_1}, b_2 = \frac{C_1 l_{f1}}{I_1}, \\ L_1 = l_{f1} + l_{r1}, L_2 = l_{f2} + l_{r2} \end{gathered} \tag{6}$$

B. Error dynamics model

This paper aims to propose a path-tracking controller for autonomous articulated vehicles. The tracking errors to the planned path were used, which were modeled using error dynamics. In particular, lateral and heading errors were used. The error dynamics consider the position of the center of gravity of the first unit relative to the planned path. The dynamics of the tracking error for the first unit can be expressed as follows:

$$\begin{aligned}\dot{\bar{e}}_{\varphi 1} &= \bar{r}_1 - \bar{v}_{x1}\kappa_{des} \\ \dot{\bar{e}}_{y1} &= \bar{v}_{y1} + \bar{v}_{x1}\bar{e}_{\varphi 1}\end{aligned} \tag{7}$$

Furthermore, the lateral error of the second unit ($\bar{e}_{y2}$) can be defined based on the prediction model, as shown in Fig. 3. The second unit's lateral error can be approximated as (8) for the planned curvature.

$$\begin{aligned}&\bar{e}_{y2} \approx \\ &\bar{e}_{y1} - (l_{r1} + P_1 + l_{f2})\bar{e}_{\varphi 1} - l_{f2}\bar{\alpha} - (l_{r1} + P_1 + l_{f2})l_{f2}\kappa_{des}\end{aligned} \tag{8}$$

C. Prediction model for tracking control

The tracking error dynamics were combined with the lumped lateral dynamics of the articulated vehicle to form a prediction model. Tracking error states ($\bar{e}_{\varphi 1}, \bar{e}_{y1}$) were augmented to the prediction model state. Finally, the tracking error prediction model of articulated vehicles is expressed as follows by combining (6) and (7).

$$\begin{gathered}\text{Let, } \bar{\mathbf{x}} = \begin{bmatrix}\bar{v}_{y1} \ \bar{r}_1 \ \bar{r}_2 \ \bar{\alpha} \ \bar{e}_{\varphi 1} \ \bar{e}_{y1}\end{bmatrix}^T, \bar{\mathbf{u}} = \bar{\delta}, \\ \bar{\mathbf{y}} = \begin{bmatrix}\bar{v}_{y1} \ \bar{r}_1 \ \bar{r}_2 \ \bar{e}_{\varphi} \ \bar{e}_{y1} \ \bar{e}_{y2}\end{bmatrix}^T, \\ \bar{\mathbf{y}}_{\mathbf{des}} = \begin{bmatrix}0 \ \bar{v}_{x1}\kappa_{des} \ \bar{v}_{x1}\kappa_{des} \ 0 \ 0 \ 0\end{bmatrix}^T \\ \dot{\bar{\mathbf{x}}} = \bar{\mathbf{A}}\bar{\mathbf{x}} + \bar{\mathbf{B}}\bar{\mathbf{u}} + \bar{\mathbf{B}}_{\mathbf{r}}\kappa_{des}, \bar{\mathbf{y}} - \bar{\mathbf{y}}_{\mathbf{des}} = \bar{\mathbf{C}}\bar{\mathbf{x}} + \bar{\mathbf{D}}\kappa_{des} \\ \text{where} \\ \bar{\mathbf{A}} = \begin{bmatrix} \multicolumn{4}{c}{} & 0 & 0 \\ \multicolumn{4}{c}{\mathbf{T_0^{-1}A_0}} & 0 & 0 \\ \multicolumn{4}{c}{} & 0 & 0 \\ \multicolumn{4}{c}{} & 0 & 0 \\ 0 & 1 & 0 & 0 & 0 & 0 \\ 1 & 0 & 0 & 0 & \bar{v}_{x1} & 0 \end{bmatrix}, \bar{\mathbf{B}} = \begin{bmatrix} \\ \mathbf{T_0^{-1}B_0} \\ \\ \\ 0 \\ 0 \end{bmatrix}, \\ \bar{\mathbf{B}}_{\mathbf{r}} = \begin{bmatrix}0 \\ 0 \\ 0 \\ 0 \\ -\bar{v}_{x1} \\ 0\end{bmatrix}, \bar{\mathbf{D}} = \begin{bmatrix}0 \\ -\bar{v}_{x1} \\ -\bar{v}_{x1} \\ 0 \\ 0 \\ -(l_{r1} + P_1 + l_{f2})l_{f2}\end{bmatrix}, \\ \bar{\mathbf{C}} = \begin{bmatrix} 1 & 0 & 0 & 0 & 0 & 0 \\ 0 & 1 & 0 & 0 & 0 & 0 \\ 0 & 0 & 1 & 0 & 0 & 0 \\ 0 & 0 & 0 & 0 & 1 & 0 \\ 0 & 0 & 0 & 0 & 0 & 1 \\ 0 & 0 & 0 & -l_{f2} & -(l_{r1} + P_1 + l_{f2}) & 1 \end{bmatrix}\end{gathered} \tag{9}$$

For the tracking reference of each output, $\bar{v}_{y1}$ is zero to ensure vehicle safety, $\bar{r}_1, \bar{r}_2$ are based on the planned curvature, and $\bar{e}_{\varphi 1}, \bar{e}_{y1}$, and $\bar{e}_{y2}$ are zero to reduce the tracking error. For ease of computation, discretization transformed the above continuous prediction model into a discrete prediction model system as (10).

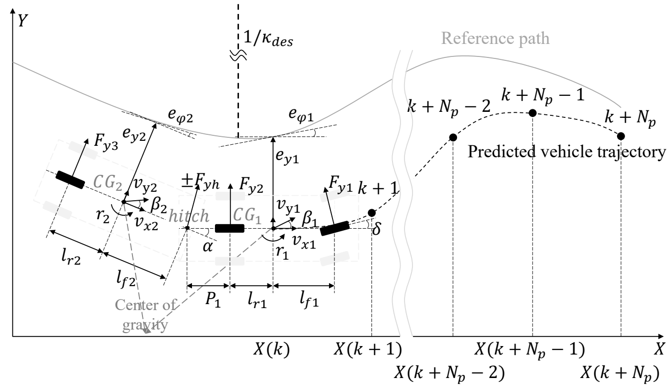

Fig. 3. Error dynamics for the planned path.

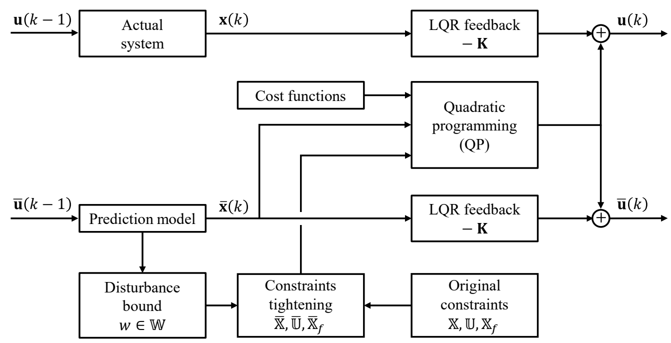

Fig. 4. Overall schematics of the proposed tracking control algorithm.

$$\begin{gathered}\bar{\mathbf{x}}(k+1) = \bar{\mathbf{A}}_{\mathbf{d},\mathbf{k}}\bar{\mathbf{x}}(k) + \bar{\mathbf{B}}_{\mathbf{d}}\bar{\mathbf{u}}(k) + \bar{\mathbf{B}}_{\mathbf{rd},\mathbf{k}}\kappa_{des}(k), \\ \bar{\mathbf{y}}(k) - \bar{\mathbf{y}}_{\mathbf{des}}(k) = \bar{\mathbf{C}}_{\mathbf{d}}\bar{\mathbf{x}}(k) + \bar{\mathbf{D}}_{\mathbf{d},\mathbf{k}}\kappa_{des}(k), \\ \\ \text{where } \bar{\mathbf{A}}_{\mathbf{d},\mathbf{k}} = \mathbf{I}_{6\times 6} + \bar{\mathbf{A}}|_{\bar{v}_{x1}=\bar{v}_{x1}(k)}\triangle t \\ \bar{\mathbf{B}}_{\mathbf{d}} = \bar{\mathbf{B}}\triangle t, \ \bar{\mathbf{B}}_{\mathbf{rd},\mathbf{k}} = \bar{\mathbf{B}}_{\mathbf{r}}|_{\bar{v}_{x1}=\bar{v}_{x1}(k)}\triangle t \\ \bar{\mathbf{C}}_{\mathbf{d}} = \bar{\mathbf{C}}, \ \bar{\mathbf{D}}_{\mathbf{d},\mathbf{k}} = \bar{\mathbf{D}}|_{\bar{v}_{x1}=\bar{v}_{x1}(k)}\end{gathered} \tag{10}$$

The longitudinal velocity of the first unit ($\bar{v}_{x1}$) varies with time. Therefore, $\bar{\mathbf{A}}_{\mathbf{d},\mathbf{k}}, \bar{\mathbf{B}}_{\mathbf{rd},\mathbf{k}}$, and $\bar{\mathbf{D}}_{\mathbf{d},\mathbf{k}}$ are modeled as time-varying matrices that change with time. In contrast, $\bar{\mathbf{B}}_{\mathbf{d}}$ and $\bar{\mathbf{C}}_{\mathbf{d}}$ are modeled as a time-invariant matrix that does not change with time because it is not affected by $\bar{v}_{x1}$

III. Proposed robust model predictive control algorithm for tracking control

This section proposes a robust tracking controller for autonomous articulated vehicles, utilizing the tube-based RMPC technique to ensure robustness. The overall schematics of the proposed algorithm are shown in Fig. 4. Throughout this chapter, the symbol $(\bar{\cdot})$ denotes the nominal states and inputs obtained from the prediction model, and $(\cdot)$ represents the actual states and inputs of the actual plant.

A. Cost functions for tracking control

The proposed tracking controller was based on MPC. The cost function for tracking the planned path was established by considering the following factors: tracking error, articulated vehicle states, and control input, with each value treated as a quadratic cost. Consequently, the cost function for path tracking is configured as follows:

$$\min_{\bar{\mathbf{U}}} J = \sum_{m=0}^{N_p-1} \|\bar{\mathbf{y}}(k+m|k) - \bar{\mathbf{y}}_{\mathbf{des}}(k+m)\|_{\mathbf{Q}} \tag{11a}$$

$$+ \sum_{m=0}^{N_c-1} \|\bar{\mathbf{u}}(k+m)\|_{\mathbf{R}} + \|\bar{\mathbf{y}}(k+N_p|k) - \bar{\mathbf{y}}_{\mathbf{des}}(k+N_p)\|_{\mathbf{P_f}}$$

$$\text{s.t. } \bar{\mathbf{x}}(k+1) = \bar{\mathbf{A}}_{\mathbf{d,k}}\bar{\mathbf{x}}(k) + \bar{\mathbf{B}}_{\mathbf{d}}\bar{\mathbf{u}}(k) + \bar{\mathbf{B}}_{\mathbf{rd,k}}\kappa_{des}(k) \tag{11b}$$

$$\bar{\mathbf{y}}(k) - \bar{\mathbf{y}}_{\mathbf{des}}(k) = \bar{\mathbf{C}}_{\mathbf{d}}\bar{\mathbf{x}}(k) + \bar{\mathbf{D}}_{\mathbf{d,k}}\kappa_{des}(k) \tag{11c}$$

Terminal cost ($\mathbf{P_f}$) and feedback gain ($\mathbf{K}$) can be calculated according to (12). $\mathbf{P_f}$, $\mathbf{K}$ are used to ensure the robustness of the algorithm. Here, the feedback gain, $\mathbf{K}$, equals to the linear quadratic regulator's (LQR) feedback gain.

$$\begin{aligned} \mathbf{P_f} &= (\bar{\mathbf{A}}_{\mathbf{d,k}} - \bar{\mathbf{B}}_{\mathbf{d}}\mathbf{K})^T \mathbf{P_f} (\bar{\mathbf{A}}_{\mathbf{d,k}} - \bar{\mathbf{B}}_{\mathbf{d}}\mathbf{K}) + \mathbf{Q} + \mathbf{K}^T\mathbf{R}\mathbf{K} \\ \mathbf{K} &:= (\bar{\mathbf{B}}_{\mathbf{d}}^T\mathbf{P_f}\bar{\mathbf{B}}_{\mathbf{d}} + \mathbf{R})^{-1}\bar{\mathbf{B}}_{\mathbf{d}}^T\mathbf{P_f}\bar{\mathbf{A}}_{\mathbf{d,k}}^T \end{aligned} \tag{12}$$

Remark 1. *The system matrix ($\bar{\mathbf{A}}_{\mathbf{d,k}}, \bar{\mathbf{B}}\mathbf{d}$) employed in this study exhibits linear time-varying characteristics that are influenced by the longitudinal velocity. While it is technically feasible to calculate and update $\mathbf{P_f}$ and $\mathbf{K}$ in real-time, doing so would introduce high computational complexity. Additionally, variations in these values can affect the robustness analysis. Therefore, this study uses fixed values of $\mathbf{P_f}$ and $\mathbf{K}$. Specifically, the maximum velocity of the ego vehicle ($100\,km/h$) is employed as the constant speed value to stabilize ($\bar{\mathbf{A}}\mathbf{d},\mathbf{k} - \bar{\mathbf{B}}_{\mathbf{d}}\mathbf{K}$).*

The covariance matrices $\mathbf{Q}$ and $\mathbf{R}$ of the cost function are specified as shown in (13).

$$\mathbf{Q} = \begin{bmatrix} \mathbf{I}_{4\times4} & \mathbf{0}_{4\times2} \\ \mathbf{0}_{2\times4} & 100\times\mathbf{I}_{2\times2} \end{bmatrix}, \mathbf{R} = 100 \tag{13}$$

Remark 2. *The covariance matrices ($\mathbf{Q}, \mathbf{R}$) determine the properties of the controller. The proposed algorithm aims to achieve precise tracking control while ensuring smooth steering. Therefore, the tracking error and input terms were assigned weights of 100, while the remaining states were assigned 1. These covariance matrices, $\mathbf{Q}, \mathbf{R}$, can be adjusted according to future control objectives.*

B. Constraints for tracking control

Constraints are essential for securing the safety of autonomous articulated vehicles and considering the performance limits of an input actuator. In addition, MPC has the advantage of being able to handle constraints easily [17]. This section introduces and applies the following four constraints among several constraints. These are set in terms of performance limits of control input actuators, lateral stability, rollover prevention, and safety, respectively.

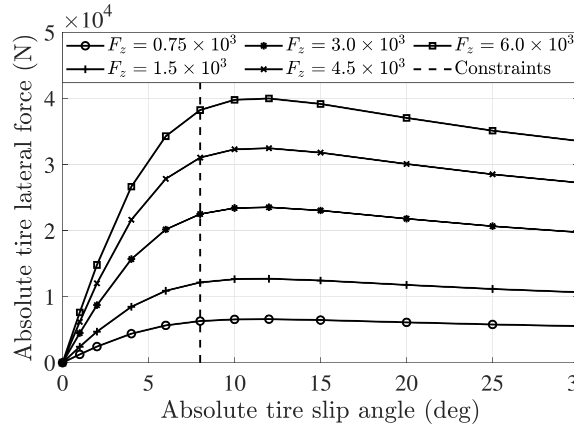

Fig. 5. Tire slip angle vs Lateral tire force.

- Input constraints

For an autonomous articulated vehicle, the steering wheel angle can rotate up to $1080\,deg$ [25]. The steering gear ratio (k_{sw}) determines the steering wheel angle (δ_{sw}) and steer angle (δ) relationship as follows:

$$\delta_{sw} = k_{sw}\delta = 25\times\delta \tag{14}$$

The following constraints were established to reflect the actuator limit.

$$\delta_{sw} \in [\delta_{sw,min},\, \delta_{sw,max}] \tag{15}$$

- Tire slip angle constraints

The tire slip angle is essential for evaluating a vehicle's lateral stability. A large side slip angle causes a loss of vehicle safety and leads to an uncontrollable. It occurs due to the lateral characteristics of the tire. Fig. 5 shows the lateral force of the tire as a function of the tire slip angle. The tire reaches full saturation when the tire slip angle surpasses $10\,deg$. The vehicle loses lateral stability at this point, and the desired steering behavior cannot be achieved. Therefore, constraints such as (16) were set for the tire slip angle of each axis.

$$\begin{aligned} \bar{\alpha}_1 &= \bar{\beta}_1 + \frac{l_{f1}}{\bar{v}_{x1}}\bar{r}_1 - \bar{\delta} \in [\alpha_{min},\, \alpha_{max}], \\ \bar{\alpha}_2 &= \bar{\beta}_1 - \frac{l_{r1}}{\bar{v}_{x1}}\bar{r}_1 \in [\alpha_{min},\, \alpha_{max}], \\ \bar{\alpha}_3 &= \bar{\beta}_2 - \frac{l_{r2}}{\bar{v}_{x2}}\bar{r}_2 \in [\alpha_{min},\, \alpha_{max}] \end{aligned} \tag{16}$$

- Lateral acceleration constraints

Heavy-duty vehicles and trucks, including articulated vehicles, have a higher center of gravity than general passenger vehicles, making them more susceptible to rollover accidents that account for many fatal crashes. Therefore, preventing rollovers in articulated vehicles is a crucial problem that needs to be addressed [29]. Among various previous approaches for preventing rollover, the simplest and most efficient method is

TABLE IV
CONSTRAINT VALUES FOR TRACKING CONTROL.

Constraint	Symbol	Value	Characteristic
Steering wheel angle	$\delta_{sw,min,max}$	$\pm 1080\,deg$	Hard constraint
Tire slip angle	$\beta_{min,max}$	$\pm 8\,deg$	Soft constraint
Lateral acceleration	$a_{y,min,max}$	$\pm 5\,m/s^2$	Soft constraint
Tracking error	$E_{min,max}$	$\pm 50\,cm$	Hard constraint

restricting the vehicle's lateral acceleration [30]. In this study, we prevent rollovers in the articulated vehicle by limiting the maximum lateral acceleration of the first and second units. Constraints for the lateral acceleration were set as follows.

$$\begin{aligned}\bar{a}_{y1} &= \bar{r}_1\bar{v}_{x1} + \dot{\bar{\beta}}_1\bar{v}_{x1} \in [a_{y,min},\, a_{y,max}],\\ \bar{a}_{y2} &= \bar{r}_2\bar{v}_{x2} + \dot{\bar{\beta}}_2\bar{v}_{x2} \in [a_{y,min},\, a_{y,max}]\end{aligned} \tag{17}$$

- Tracking error constraints for collision avoidance

Autonomous articulated vehicles, the target plants in this study, have a wider width than passenger cars. Considering the typical lane width ($3.5\,m \sim 4.0\,m$) [31] and the ego vehicle width ($2.5\,m$) [25], there is only about $0.5 \sim 0.75\,m$ of clearance on both sides of the vehicle. If the boundary of the tracking error exceeds this range, the ego vehicle may cross the lane or collide with an obstacle. Hence, it is essential to establish appropriate tracking error constraints to ensure safe driving. Additionally, as articulated vehicles consist of multiple units, it is crucial to guarantee the tracking error for both the first and second units. The prediction model employed in this study enables the prediction of tracking errors for both the first and second units. Therefore, constraints for the two units' tracking errors can be set. In this study, a tracking error boundary of $\pm 50\,cm$ ($E_{min,max}$) was selected, taking into account the vehicle's width and dimensions. These constraints can be defined as follows:

$$\begin{aligned}e_{y1} &\in [E_{min},\, E_{max}],\\ e_{y2} &\in [E_{min},\, E_{max}]\end{aligned} \tag{18}$$

Finally, four constraints have been introduced. Table IV presents each constraint's minimum and maximum values. It is important to note that the impact on stability and safety varies even if a constraint is slightly exceeded. For instance, exceeding a limited value for the tire slip angle may not wholly compromise the stability or safety of the entire system. Such constraints that allow slight exceedance are referred to as soft constraints.

On the other hand, if the tracking errors exceed the constraints, critical situations like lane crossing and obstacle collisions may arise. In other words, these constraints must be unconditionally satisfied and are referred to as hard constraints. The characteristics of each constraint are outlined in Table IV as well. When ensuring robustness against modeling errors, considering all conditions as hard constraints would result in highly conservative control outcomes. Hence, it is reasonable to proceed with constraint tightening for modeling errors only for hard constraints.

C. Tube-based robust model predictive control

MPC relies on prediction models to forecast future behavior, but errors between the prediction model and the actual plant are unavoidable. These modeling errors can impact performance, robustness, and stability. Tube-based RMPC addresses this issue by analyzing the maximal error set resulting from modeling errors. It then tightens the constraints based on this analysis to ensure robustness.

This study utilizes multiple sets, and operations such as Minkowski set addition, subtraction, and multiplication are defined and applied as follows:

Definition 1.

$$\begin{aligned}\textit{Set addition}\,:& X \oplus Y := \{x+y \mid x \in X, y \in Y\}\\ \textit{Set subtraction}\,:& X \ominus Y := \{z \mid z \oplus Y \subseteq X\}\\ \textit{Set multiplication}\,:& \textit{Let } \mathbf{K} \in \mathbb{R}^{m\times n},\, \mathbf{K}X := \{\mathbf{K}x \mid x \in X\}\end{aligned} \tag{19}$$

The addictive disturbance represents the modeling error between the prediction model and the actual plant, $\mathbf{w}(k)$, as follows:

$$\begin{aligned}\bar{\mathbf{x}}(k+1) &= \mathbf{A}\bar{\mathbf{x}}(k) + \mathbf{B}\bar{\mathbf{u}}(k)\\ \mathbf{x}(k+1) &= \mathbf{A}\mathbf{x}(k) + \mathbf{B}\mathbf{u}(k) + \mathbf{w}(k)\end{aligned} \tag{20}$$

Tube-based RMPC assumed that $\mathbf{w}(k)$ is bounded. Here, $\mathbb{W}$ denotes the maximum disturbance set.

$$\mathbf{w}(k) \in \mathbb{W},\, \forall k \tag{21}$$

In tube-based RMPC, the actual input consists of nominal input and feedback input as (22) to ensure robustness.

$$\mathbf{u}(k) = \bar{\mathbf{u}}(k) - \mathbf{K}(\mathbf{x}(k) - \bar{\mathbf{x}}(k)) \tag{22}$$

where $\mathbf{K}$ is the feedback gain, which calculated using (12). The error propagation of tube-based RMPC with the feedback controller added is as follows:

$$\begin{aligned}&\mathbf{e}(k+m) = \sum_{i=0}^{m-1}\left(\mathbf{A_K}^{m-1-i}\mathbf{w}(k+i)\right)\\ &\text{where } \mathbf{e}(k+m) = \mathbf{x}(k+m) - \bar{\mathbf{x}}(k+m),\, \mathbf{A_K} = \mathbf{A} - \mathbf{BK}\end{aligned} \tag{23}$$

In the tube-based RMPC technique, as shown in (23), the error is propagated by the closed-loop matrix ($\mathbf{A_K}$) instead of the system matrix ($\mathbf{A}$). Hence, incorporating feedback input stabilizes errors and ensures the system's robustness [32]. The error tube represents the maximal set within which errors can exist at each step. By employing (21) and (23), the error tube for each step can be defined as follows:

$$\begin{aligned}&\mathbf{e}(k+m) \in S_m\\ &\text{where } S_m := \sum_{i=0}^{m-1}\mathbf{A_K}^{m-1-i}\mathbb{W} = \mathbf{A_K}^{m-1}\mathbb{W} \oplus \cdots \oplus \mathbb{W}\end{aligned} \tag{24}$$

Since the feedback gain ($\mathbf{K}$) stabilizes the system, $\mathbf{A_K}$ is always stable. Therefore, S_m always converges due to the feedback gain as follows:

$$S_\infty := \sum_{i=0}^{\infty} \mathbf{A_K}^i \mathbb{W} = \mathbb{W} \oplus \mathbf{A_K}\mathbb{W} \oplus \dots \tag{25}$$

The original hard constraints the controller must unconditionally satisfy can be expressed as follows:

$$\begin{aligned} &\mathbf{x}(k+m|k) \in \mathbb{X}, && m = 0, \cdots, N_p - 1 \\ &\mathbf{x}(k+m|k) \in \mathbb{X}_f, && m = N_p \\ &\mathbf{u}(k+m) \in \mathbb{U}, && m = 0, \cdots, N_c - 1 \end{aligned} \tag{26}$$

where $\mathbb{X}$ represents state constraints, $\mathbb{X}_f$ represents terminal constraints, and $\mathbb{U}$ represents input constraints. Constraint tightening ensures that equation (26) is satisfied even with modeling error. To achieve this, we introduce tightened nominal state and input constraints based on (25).

$$\begin{aligned} &\bar{\mathbf{x}}(k+m|k) \in \bar{\mathbb{X}}, && m = 0, \cdots, N_p - 1 \\ &\bar{\mathbf{x}}(k+m|k) \in \bar{\mathbb{X}}_f, && m = N_p \\ &\bar{\mathbf{u}}(k+m) \in \bar{\mathbb{U}}, && m = 0, \cdots, N_c - 1 \\ &\text{where } \bar{\mathbb{X}} = \mathbb{X} \ominus S_\infty, \, \bar{\mathbb{X}}_f = \mathbb{X}_f \ominus S_\infty, \, \bar{\mathbb{U}} = \mathbb{U} \ominus \mathbf{K}S_\infty \end{aligned} \tag{27}$$

If the condition (27) for nominal states and inputs is satisfied, then the corresponding condition (26) for actual states and inputs are automatically satisfied according to the definition of S_∞. In conclusion, the original constraints can always be satisfied even with modeling error through constraints tightening based on the error tube, which guarantees robustness.

This study established hard constraints for input and tracking error, as presented in Table IV. To ensure robustness, we employed a constraints-tightening technique to reset the expressions (15) and (18) as follows:

$$\begin{aligned} &\delta_{sw} \in [\delta_{sw,min},\, \delta_{sw,max}] \ominus k_{sw}\mathbf{K}S_\infty \\ &e_{y1} \in [E_{min},\, E_{max}] \ominus \mathbf{C}_1 S_\infty, \\ &e_{y2} \in [E_{min},\, E_{max}] \ominus \mathbf{C}_2 S_\infty \\ &\text{where } \mathbf{C}_1 = [0\ \ 0\ \ 0\ \ 0\ \ 0\ \ 1], \\ &\mathbf{C}_2 = [0\ \ 0\ \ 0\ \ -l_{f2}\ \ -(l_{r1} + P_1 + l_{f2})\ \ 1] \end{aligned} \tag{28}$$

Finally, the proposed robust tracking controller for autonomous articulated vehicles is presented as follows.

$$\min_{\bar{\mathbf{U}}} \text{(11a)}, \quad \text{s.t. (11b), (11c), (16), (17), (28)} \tag{29}$$

IV. Error tube analysis for autonomous articulated vehicles

A. Simulation environments

This study analyzed modeling errors using the TruckSim simulation software and proposed a robust controller. TruckSim offers precise simulation capabilities by employing a high degree-of-freedom model for articulated vehicles. The articulated bus, a type of articulated vehicle, was used in the simulation. The specification of the used articulated bus is identical to an actual one as presented in Table II.

Fig. 6. Articulated bus and experimental setup.

TABLE V
Similarity between experiment and simulation.

States	RMSE	NRMSE
Articulated angle	$0.383\,deg$	7.64%
Yaw rate: First unit	$0.608\,deg/s$	6.19%
Yaw rate: Second unit	$0.922\,deg/s$	8.99%
Lateral acceleration: First unit	$0.274\,m/s^2$	10.05%
Lateral acceleration: Second unit	$0.269\,m/s^2$	8.86%

Before the simulations, a comprehensive evaluation was conducted to assess the depiction of the simulated vehicle compared to the actual vehicle. The experimental setup is shown in Fig. 6, where two RT devices were attached to the articulated bus to measure the actual sensor signals. In this evaluation, the actual vehicle and TruckSim sensor signals were compared and analyzed during three double-lane-change maneuvers at a speed of $60\,kp/h$. The test results from the actual vehicle and the simulation results for the same maneuver are shown in Fig. 7. Specifically, the evaluation focused on the similarity of crucial factors influencing lateral behavior: yaw rate, lateral acceleration, and articulated angle.

The similarity was quantitatively assessed using root mean square error (RMSE) and normalized RMSE (NRMSE). RMSE and NRMSE for each state are analyzed as follows:

$$\text{RMSE} := \|(\cdot)_{act} - (\cdot)_{sim}\|, \quad \text{NRMSE} := \frac{\|(\cdot)_{act} - (\cdot)_{sim}\|}{\max(|(\cdot)_{act}|)} \tag{30}$$

where $(\cdot)_{act}$ and $(\cdot)_{sim}$ represent the states measured by experiments and simulations, respectively. The analysis results are shown in Table V. The simulation conducted through TruckSim exhibited a similarity of about 90% across all vehicle states. The minor disparities observed can be attributed to the imperfect measurement of parameters such as toe and camber in the actual vehicle. More accurate simulations can be achieved with complete knowledge of all component parameters. Nevertheless, the simulated environment by TruckSim provides a sufficiently accurate representation of the actual vehicle for analyzing the proposed algorithm.

B. Maximal error tube: Prediction model vs Actual plant

This section analyzes the maximal error tube between the prediction model and the actual plant, simulated in TruckSim.

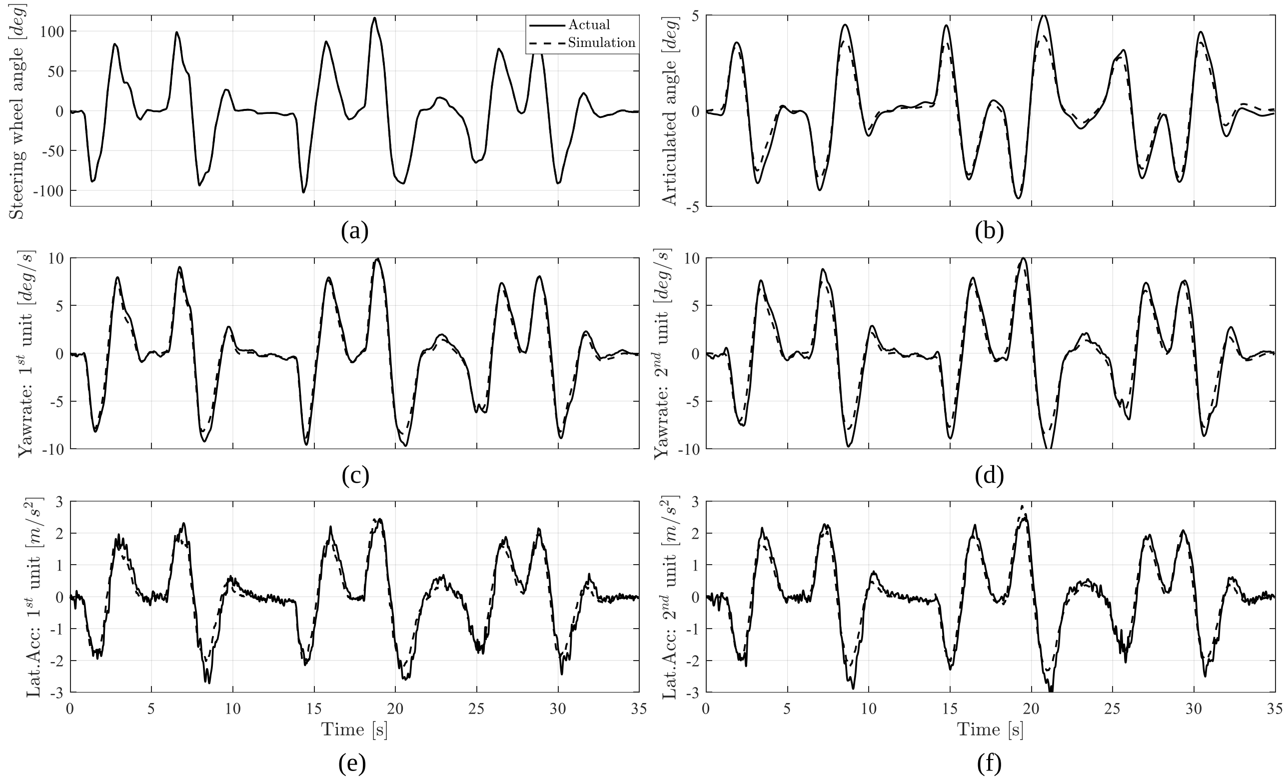

Fig. 7. Actual articulated vehicle test results vs Simulation results. (a) Steering wheel angle. (b) Articulated angle. (c) Yaw rate of the first unit. (d) Yaw rate of the second unit. (e) Lateral acceleration of the first unit. (f) Lateral acceleration of the second unit.

The prediction model, actual plant, and disturbance are shown in (31).

$$\begin{aligned}\bar{\mathbf{x}}(k+1) &= \bar{\mathbf{A}}_{\mathbf{d},\mathbf{k}}\bar{\mathbf{x}}(k) + \bar{\mathbf{B}}_{\mathbf{d}}\bar{\mathbf{u}}(k) + \bar{\mathbf{B}}_{\mathbf{rd},\mathbf{k}}\kappa_{des}(k) \\ \mathbf{x}(k+1) &= \bar{\mathbf{A}}_{\mathbf{d},\mathbf{k}}\mathbf{x}(k) + \bar{\mathbf{B}}_{\mathbf{d}}\mathbf{u}(k) + \bar{\mathbf{B}}_{\mathbf{rd},\mathbf{k}}\kappa_{des}(k) + \mathbf{w}(k)\end{aligned} \tag{31}$$

In order to obtain the maximal error tube, it is essential to analyze the disturbance boundary ($\mathbb{W}$) of the disturbance ($\mathbf{w}$). We calculated S_∞ under various deceleration, acceleration, and steering scenarios. The corresponding scenario used in this study is illustrated in Fig. 8.

At each step, $S_{\infty,k}$ was analyzed through the following process:

1. Identifying maximum disturbance at k step: $\mathbf{w}(k) \in \mathbb{W}_k$
2. Identifying system matrices for $\bar{v}_x(k)$ at k step: $\bar{\mathbf{A}}_{\mathbf{d},\mathbf{k}}, \bar{\mathbf{B}}_{\mathbf{d},\mathbf{k}}$
3. Set feedback control gain at $100 km/h$ (stable gain): $\mathbf{K}$

We used fixed LQR feedback gain at the maximum velocity of $100\, km/h$. If $\mathbf{K}$ is defined at a lower velocity than the maximum velocity, the closed-loop system ($\bar{\mathbf{A}}_{\mathbf{d},\mathbf{k}} - \bar{\mathbf{B}}_{\mathbf{d},\mathbf{k}}\mathbf{K}$) becomes unstable at higher velocities. Therefore, we defined $\mathbf{K}$ at the maximum velocity, $100\, km/h$.

4. Analyzing maximal error tube at k step ($S_{\infty,k}$) as follows:

$$\begin{aligned}S_{\infty,k} := &\sum_{i=0}^{\infty}(\bar{\mathbf{A}}_{\mathbf{d},\mathbf{k}} - \bar{\mathbf{B}}_{\mathbf{d},\mathbf{k}}\mathbf{K})^i\mathbb{W} \\ =&\mathbb{W} \oplus (\bar{\mathbf{A}}_{\mathbf{d},\mathbf{k}} - \bar{\mathbf{B}}_{\mathbf{d},\mathbf{k}}\mathbf{K})\mathbb{W}_k \oplus \dots\end{aligned} \tag{32}$$

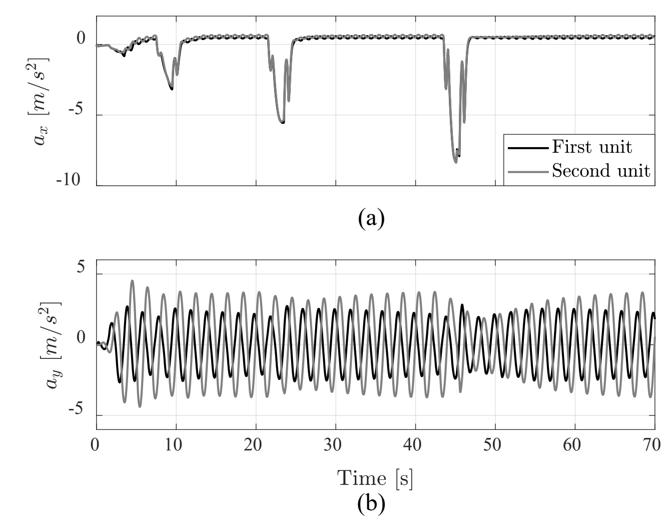

Fig. 8. Scenario of maximal disturbance analysis. (a) Longitudinal acceleration. (b) Lateral acceleration.

5. Analyzing maximal error tube as follows:

$$S_\infty := \max(S_{\infty,k}) \tag{33}$$

The maximal error tubes of the lateral error for the first unit ($\bar{e}_{y2}$) and second unit ($\bar{e}_{y1}$) through (32) and (33) for various conditions are shown in Fig. 9.

For Fig. 9, the X-axis represents the error propagation step, while the Y-axis represents the maximum size of the maximal

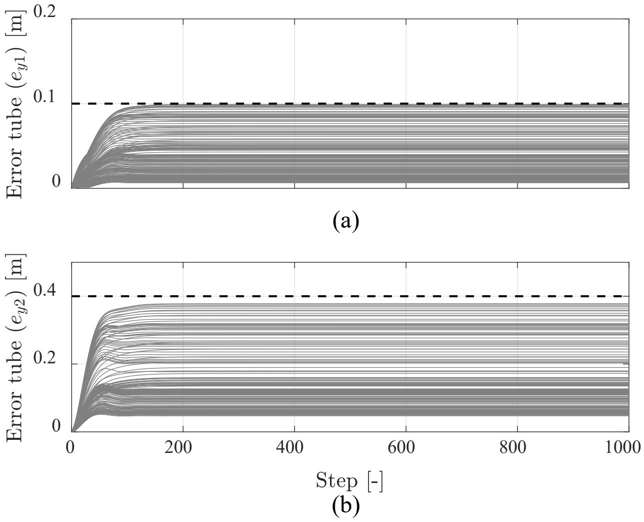

Fig. 9. Maximal error tube of lateral errors. (a) First unit. (b) Second unit.

TABLE VI
MAXIMAL ERROR TUBES & CONSTRAINT TIGHTENING.

	Original constraints	Maximal error tube	Tightened constrains
$e_{y1}[m]$	$[-0.5, 0.5]$	$[-0.1, 0.1]$	$[-0.4, 0.4]$
$e_{y2}[m]$	$[-0.5, 0.5]$	$[-0.4, 0.4]$	$[-0.1, 0.1]$
$\delta_{sw}[deg]$	$[-1080, 1080]$	$[-30, 30]$	$[-1050, 1050]$

error tube. Fig. 9 shows that the maximal lateral error for the first unit is within $10\,cm$, and the maximal lateral error for the second unit is within $40\,cm$. These values represent the maximum error boundary for a disturbance, including modeling error, can cause. Furthermore, the maximal feedback input tube ($k_{sw}\mathbf{K}S_\infty$) is within $30\,deg$ for the steering wheel angle. Finally, the input and tracking error constraints were tightened by conducting error tube analysis, as presented in Table VI.

Remark 3. *The tube-based RMPC employs a constraints tightening approach* $((\bar{\mathbb{X}}, \bar{\mathbb{U}})->(\mathbb{X} \ominus S_\infty, \mathbb{U} \ominus \mathbf{K}S_\infty))$ *to ensure robustness against modeling errors. The constraints are set conservatively, aligned with the maximal error tube (S_∞). Consequently, a more extensive maximal error tube set might compromise the feasibility of the MPC. Fortunately, there exist several strategies to address or mitigate this issue:*

1) Accurate modeling: At its core, the discrepancy between the actual plant and the prediction model induces infeasibility. Hence, achieving accurate modeling stands as a foundational solution. 2) Hard/Soft constraints: Infeasibility primarily arises from hard constraints. Enhancing feasibility involves categorizing states as soft or hard constraints based on their criticality to the system. 3) Small/Large feedback gain: The closed-loop system matrix, $\bar{\mathbf{A}}_{\mathbf{d},\mathbf{k}} - \bar{\mathbf{B}}_{\mathbf{d},\mathbf{k}}\mathbf{K}$, *influences the maximal error tube. A large feedback gain reduces (S_∞), and a small one reduces $\mathbf{K}S_\infty$. Therefore, feasibility can be increased by adjusting the appropriate feedback gain. 4. Stochastic RMPC: Stochastic RMPC expresses error stochastically. So, although it may not satisfy original constraints 100%, it has the advantage of being less conservative. The corresponding technique can be used if it is difficult to secure the problem's feasibility.*

Employing the methods above contributes to enhancing the feasibility of the algorithm.

Remark 4. *This study analyzes modeling errors between the actual plant (simulation high-order model) and the prediction model (linear dynamics model). During this analysis, the considered disturbances are broadly categorized into three types: 1) Unmodeled dynamics, encompassing aspects like chassis and roll pitch dynamics; 2) Nonlinear tire models and complex dynamics, such as coordinate conversion; and 3) Dynamic errors arising from parameter errors. Consequently, the algorithm's robustness was secured by scrutinizing the maximum error set brought about by disturbances, including modeling inaccuracies.*

TABLE VII
TUNING PARAMETERS OF THE TRACKING CONTROLLER.

Symbol	Parameters	Value
$\triangle t$	Sampling time	$20\,ms$
N_p	Prediction horizon	100
N_c	Control horizon	100

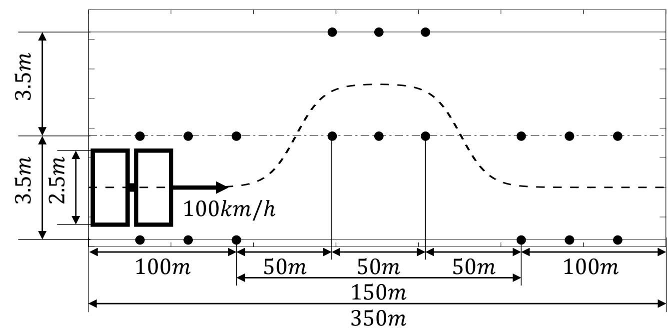

Fig. 10. Reference path: Double lane change at $100\,km/h$.

V. SIMULATION RESULTS

A. Simulation scenario & Comparison algorithm

The performance of the proposed algorithm was evaluated using the TruckSim simulation software. Tuning parameters for the proposed algorithm are shown in Table VII. The driving scenario is a double lane change (DLC) maneuver for autonomous articulated vehicles at $100\,km/h$. This particular scenario exhibits highly demanding behavior, necessitating advanced control technology to ensure the safety and stability of the vehicle. Thus, the effectiveness of the proposed algorithm can be objectively and thoroughly analyzed through this scenario. The reference path is depicted in Fig. 10.

The proposed algorithm's steering wheel angle is optimized by solving the optimization problem (29) for the reference path during the DLC maneuver. The proposed tracking controller ensures performance, safety, and robustness through the tube-based RMPC technique.

The proposed algorithm was compared and analyzed with two state-of-the-art control algorithms for tracking control.

- Linear quadratic regulator (LQR) controller

The LQR controller is an optimal control technique, exhibiting two significant distinctions from MPC. Firstly, the LQR controller generates inputs solely based on the current state without considering future reference. Secondly, it can not set states and input constraints. Hence, the strengths and attributes of the proposed algorithm are examined by conducting a comparative analysis. The control input from the LQR controller can be expressed as follows:

$$\begin{aligned} &\mathbf{u}(k) = -\mathbf{K}(\mathbf{x}(k) - \mathbf{x_{des}}(k)) \\ &\text{where } \mathbf{x}(k) - \mathbf{x_{des}}(k) = \mathbf{x}(k) + \bar{\mathbf{C}}^{-1}\bar{\mathbf{D}}\kappa_{des}(k) \end{aligned} \tag{34}$$

Here, the feedback control gain, denoted as $\mathbf{K}$, is determined through (12).

- Pursuit controller using an adaptive look-ahead

The performance of the proposed algorithm was compared with the latest geometric controller, the pure pursuit controller using an adaptive look-ahead algorithm [33]. This algorithm represents an advancement over the traditional pure pursuit algorithm and has shown superior performance among classic control algorithms. The algorithm incorporates a look-ahead distance, which is defined as:

$$l_d = (k_1 v_{x1} - l_{d,min})e^{-k_2 y_{e1}^2} + l_{d,min} \tag{35}$$

where $l_{d,min}$ represents the minimal look-ahead distance, y_{e1} represents the tracking error of the first unit, and k_1 and k_2 represent positive constants that adjust the sensitivity to speed and error. The classic tracking control algorithm was implemented by incorporating the above adaptive look-ahead distance.

B. Simulation results

The simulation results are presented in Fig. 11. In all figures, blue lines represent the proposed tube-based RMPC-based tracking controller. In contrast, red lines represent the LQR controller, and yellow lines represent the pure pursuit controller with adaptive look-ahead distance. Fig. 11(a) presents the trajectory of the autonomous articulated vehicle using each controller. The solid line represents the trajectory of the first unit, and the dash-single dotted line represents the trajectory of the second unit. The black dashed line depicts the reference path. The proposed algorithm, employing the tube-based RMPC control technique, achieves highly accurate tracking of the reference path without any lane violation. This accomplishment is particularly significant given the challenges of steering an articulated vehicle. Moreover, the trajectories of both the first and second units exhibit remarkable similarities.

In contrast, utilizing the pure pursuit method demonstrates inferior tracking performance. The occurrence of lane violations at approximately $150m$ and $250m$ can be observed, and a notable disparity between the trajectories of the first and second units is evident. Even the LQR controller, an optimization-based control approach, the second unit was observed nearly encroaching upon the lane at the $150\,m$ and $250\,m$ sections. Thus, in terms of the safety of autonomous vehicles, the tube-based RMPC approach offers significant advantages.

Fig. 11(b) presents the steering wheel angle applied by each controller. The dotted line represents the nominal input value obtained through the optimization problem in (29), while the solid line represents the actual input. The dash-single dotted line represents the feedback input by the tube-based RMPC technique. The proposed algorithm combines the nominal input and the feedback input to form the actual input. The nominal input optimizes the cost function, while the feedback input ensures robustness against disturbances. As a result, the proposed algorithm guarantees both optimization and robustness. Notably, the proposed algorithm requires significantly lower input compared to LQR and pure pursuit controllers. Despite the lower input value, the proposed algorithm ensures higher performance and robustness than pure pursuit.

Fig. 11(c) presents the yaw rate of the autonomous articulated vehicle. The solid line represents the result for the first unit, while the dash-single dotted line represents the result for the second unit. Like the steering wheel angle, the proposed algorithm exhibits a relatively low yaw rate, whereas the LQR and pure pursuit controllers demonstrate a considerably higher yaw rate. The proposed algorithm achieves high tracking performance even with a low yaw rate.

Fig. 11(d)-(e) present the tracking errors of the first and second units, respectively. The blue dotted line represents the nominal tracking error obtained through optimization in (29), while the solid line represents the actual tracking error. For the target system, the maximum allowable tracking error was set to $50\,cm$, considering the vehicle width and lane width, and the black dotted line represents these original constraints. These are hard constraints that must always be satisfied. Therefore, constraint tightening was performed through error tube analysis to ensure robustness, and the black dash-single dotted line represents tightened constraints. The nominal tracking error of the proposed algorithm satisfies the tightened constraints, and the actual tracking error automatically satisfies the original constraints. As a result, the proposed algorithm satisfies the original constraints, even in modeling errors.

An intriguing observation emerged from the LQR controller results. While the LQR controller demonstrated satisfactory tracking performance for the first unit, it exhibited subpar tracking performance for the second unit. Consequently, the tracking error for the second unit exceeded $50\,cm$, violating its safety constraints. It implies that while the tracking controller employing LQR can ensure performance for passenger vehicles, which are single-unit vehicles, it is necessary to apply advanced control techniques for articulated vehicles, which are multi-unit vehicles.

Also pure pursuit exhibits a tracking error exceeding $50\,cm$. Such a tracking error can lead to lane violations and collisions with obstacles, undermining safety. In fact, due to such tracking errors, lane violations occur when control is performed using pure pursuit, as shown in Fig. 11(a).

Fig. 11(f) presents the lateral acceleration. The solid line and the dash-single dotted line represent the results for the first and second units, respectively. The black dotted line indicates the original constraints. Articulated vehicles typically have a

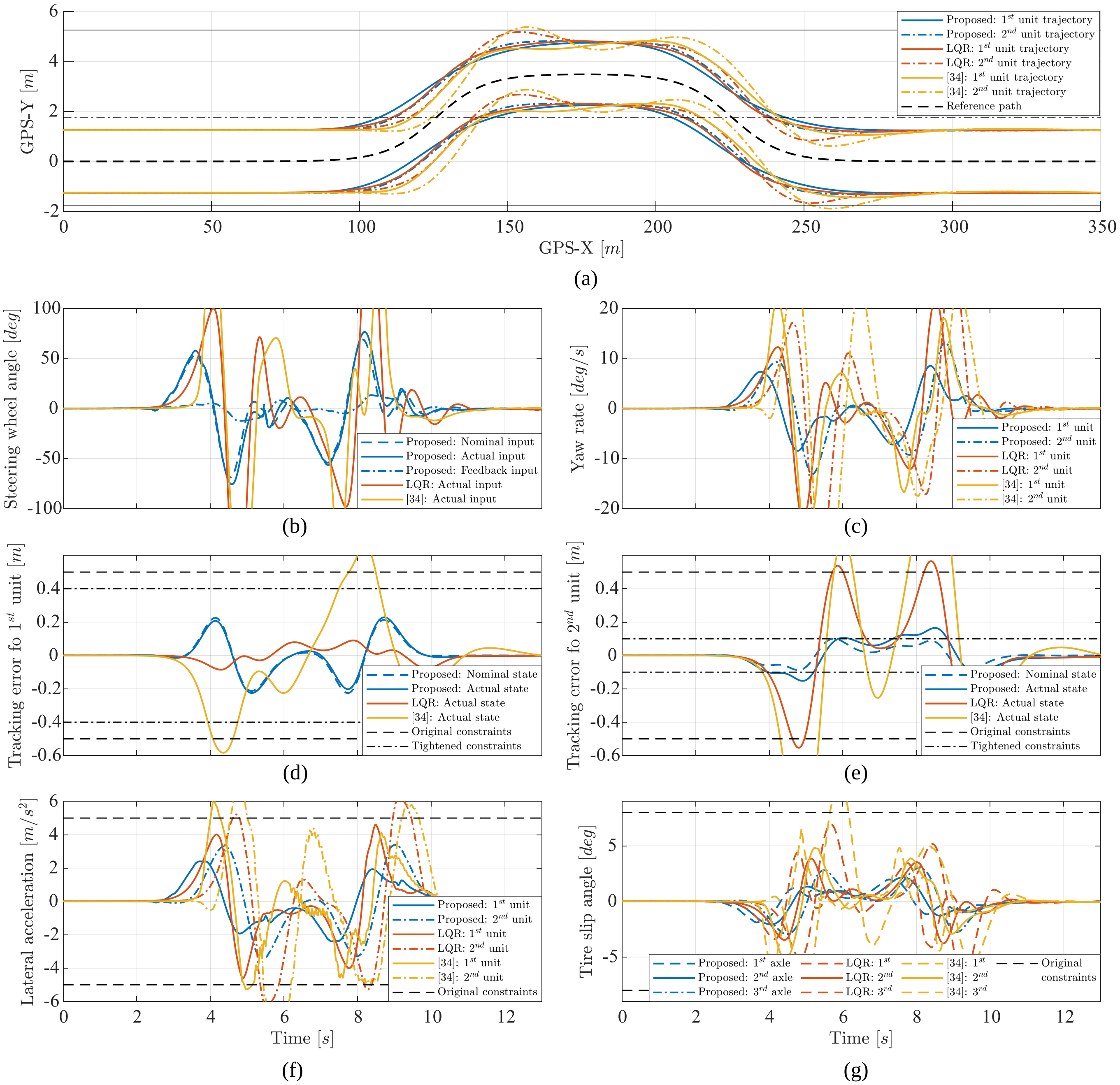

Fig. 11. Simulation results of double lane change at $100\,km/h$. (a) Trajectories of autonomous articulated vehicles. (b) Steering wheel angle. (c) Yaw rate. (d) Tracking error of the first unit. (e) Tracking error of the second unit. (f) Lateral acceleration. (g) Tire slip angle.

TABLE VIII
SIMULATION RESULTS: CONSTRAINTS, MIN., MAX. VALUES AND SATISFACTION.

			Proposed algorithm		LQR		[34]	
States	Units	Constraints	Min., Max. value	Satisfaction	Min., Max. value	Satisfaction	Min., Max. value	Satisfaction
δ_{sw}	$[deg]$	$[-1080, 1080]$	$[-138.3, 138.0]$	O	$[-220.7, 213.9]$	O	$[-307.0, 247.1]$	O
r_1	$[deg/s]$	-	$[-11.0, 11.1]$	-	$[-22.2, 21.9]$	-	$[-27.0, 21.5]$	-
r_2	$[deg/s]$	-	$[-13.1, 13.2]$	-	$[-31.1, 30.9]$	-	$[-41.3, 26.4]$	-
e_{y1}	$[m]$	$[-0.5, 0.5]$	$[-0.225, 0.229]$	O	$[-0.086, 0.090]$	O	$[-0.775, 0.776]$	X
e_{y2}	$[m]$	$[-0.5, 0.5]$	$[-0.157, 0.173]$	O	$[-0.554, 0.566]$	X	$[-1.226, 1.197]$	X
a_{y1}	$[m/s^2]$	$[-5, 5]$	$[-2.68, 2.67]$	O	$[-4.61, 4.61]$	O	$[-5.28, 6.10]$	X
a_{y2}	$[m/s^2]$	$[-5, 5]$	$[-3.40, 3.39]$	O	$[-6.17, 6.16]$	X	$[-7.59, 6.91]$	X
$\alpha_{1,2,3}$	$[deg]$	$[-8, 8]$	$[-2.94, 3.02]$	O	$[-6.88, 6.95]$	O	$[-7.98, 10.68]$	X

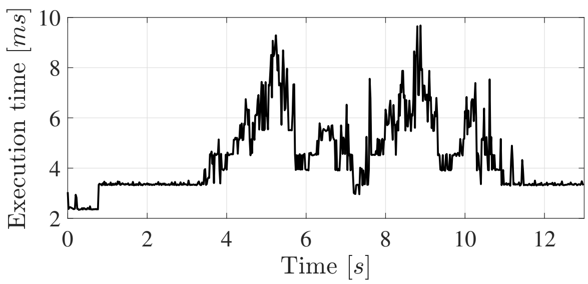

Fig. 12. Execution time of the proposed algorithm.

lateral acceleration limit of $5\,m/s^2$ to prevent rollover [30]. The proposed algorithm achieves a lateral acceleration of about $3\,m/s^2$. In contrast, the LQR and pure pursuit controllers exhibit a value exceeding $5\,m/s^2$, which can lead to a rollover. The proposed algorithm improves safety, particularly rollover prevention, through constraints on lateral acceleration.

Fig. 11(g) presents the tire slip angle for each axis. The dotted, solid, and dash-single dotted lines represent the tire slip values for the first, second, and third axes, respectively. The black dotted line depicts the original constraints. As shown in Fig. 5, tires saturate at a tire slip angle of approximately $10\,deg$. When the tires reach saturation, control actions such as braking and steering become less effective, and stability is compromised. Thus, tire slip directly affects vehicle stability and safety. The proposed algorithm prevents tire saturation by imposing constraints on tire slip angles. Also, the optimization-based LQR controller luckily satisfied the tire slip constraints. In contrast, classic controllers like pure pursuit can not consider these constraints, resulting in almost saturated tire slip angles. This property is a significant drawback in terms of stability.

Table VIII summarizes whether the constraints are satisfied and provides each state's maximum and minimum values. The proposed algorithm satisfies all constraints. In contrast, the LQR and geometric controllers violate several constraints.

Consequently, LQR and geometric controllers, including a pure suit, are unsuitable for articulated vehicles, and an advanced tracking controller such as MPC is required. Moreover, states that significantly impact safety, such as tracking errors, must be unconditionally satisfied despite modeling errors. This study proposed a robust tracking controller for autonomous articulated vehicles. In conclusion, the proposed algorithm ensures performance, safety, and robustness.

Remark 5. *'OSQP solver' [34] is used as a quadratic programming solver. This solver is a state-of-the-art algorithm. Fig. 12 presents the execution time of the proposed algorithm implemented using 'OSQP solver'. The computations were performed on an Intel Core i7-7700k CPU @ 4.20Hz. The simulation results revealed that the average execution time was* $4.44\,ms$*, much shorter than the* $20\,ms$ *sampling time. Furthermore, the maximum execution time was below* $10ms$*. Consequently, the real-time implementation of the proposed algorithm would be possible.*

VI. Conclusion and Future Work

This paper presents a novel framework for a robust tracking controller designed specifically for autonomous articulated vehicles using a tube-based RMPC approach. The proposed controller leverages the lumped lateral dynamics model as the prediction model, allowing tracking errors of first and second units to be predicted. A set of constraints was established to ensure the safety and stability of the ego vehicle. Among these constraints, certain ones were categorized as hard constraints that necessitate unconditional satisfaction. Therefore, compensation was required due to unavoidable modeling errors between the actual plant and the prediction model. This paper analyzes the maximal error tube and employs constraints tightening based on this analysis to ensure robustness. The proposed algorithm demonstrated superior performance, safety, and robustness through simulations compared to geometric controllers. The simulation results showcase the effectiveness of the proposed algorithm in accurately tracking a reference path, providing precise steering control, and adhering to safety constraints such as lateral stability, rollover prevention, and tracking error limits. The proposed framework offers significant advancements in autonomous articulated vehicles, enabling enhanced control capabilities and addressing the challenges posed by modeling errors.

While the proposed framework provides promising results, there are several avenues for future research and improvement. First, the proposed algorithm can be experimentally verified with autonomous articulated vehicles. These validations provide valuable insight into the algorithm's performance in real-world scenarios and help validate its effectiveness. It includes implementing the controller in a vehicle and conducting field tests under various driving conditions. Second, various prediction models can be combined. In particular, incorporating longitudinal dynamics could enhance the algorithm's realism and generality. Furthermore, including constraints on engine and brake torque would be beneficial. Significant future research involves the development of an integrated tracking controller that accounts for both longitudinal and lateral dynamics. In conclusion, the proposed framework for a robust tracking controller for autonomously articulated vehicles shows excellent potential to improve the safety and performance of these vehicles. Future work may focus on validating the algorithm in real-world scenarios and extending the model.

Acknowledgment

This research was partly supported by the BK21 FOUR Program of the National Research Foundation Korea(NRF) grant funded by the Ministry of Education(MOE)., the Technology Innovation Program (20014983, Development of autonomous chassis platform for a modular vehicle) funded By the Ministry of Trade, Industry & Energy(MOTIE, Korea)., and the Autonomous Driving Technology Development Innovation Program (20018181, Development of Lv. 4+ autonomous driving vehicle platform based on point-to-point driving to logistic center for heavy trucks) funded by the Ministry of Trade, Industry & Energy(MOTIE, Korea) and Korea Evaluation Institute of Industrial Technology(KEIT)

References

[1] S. Oikawa, Y. Matsui, N. Kubota, S. Aomura, K. Sorimachi, A. Imanishi, and T. Fujimura, "Features of fatal truck accidents compared with sedans," *International journal of automotive technology*, vol. 22, pp. 931–939, 2021.

[2] A. Reński, "Investigation of the influence of the centre of gravity position on the course of vehicle rollover," in *Proceedings of the 24th International Technical Conference on the Enhanced Safety of Vehicles (ESV) National Highway Traffic Safety Administration, Gothenburg, Sweden*, 2015, pp. 8–11.

[3] A. Matteson, L. Jarossi, and J. Woodrooffe, "Buses involved in fatal accidents factbook 2008," University of Michigan, Ann Arbor, Transportation Research Institute, Tech. Rep., 2011.

[4] A. Rahimi and Y. He, "A review of essential technologies for autonomous and semi-autonomous articulated heavy vehicles," in *Proceedings of the Canadian Society for Mechanical Engineering International Congress*, 2020, pp. 21–24.

[5] McKinsey., "Routh 2030: The fast track to the future commercial vehicle industry." 2018.

[6] Y. Wang, Z. Wang, K. Han, P. Tiwari, and D. B. Work, "Gaussian process-based personalized adaptive cruise control," *IEEE Transactions on Intelligent Transportation Systems*, vol. 23, no. 11, pp. 21 178–21 189, 2022.

[7] Y. Jeong, "Interactive lane keeping system for autonomous vehicles using lstm-rnn considering driving environments," *Sensors*, vol. 22, no. 24, p. 9889, 2022.

[8] D. Jeong and S. B. Choi, "Efficient trajectory planning for autonomous vehicles using quadratic programming with weak duality," *IEEE Transactions on Intelligent Vehicles*, 2023.

[9] Z. Huang, W. Lan, and X. Yu, "A formal control framework of autonomous vehicle for signal temporal logic tasks and obstacle avoidance," *IEEE Transactions on Intelligent Vehicles*, 2023.

[10] D. Jeong and S. B. Choi, "Tracking control based on model predictive control using laguerre functions with pole optimization," *IEEE Transactions on Intelligent Transportation Systems*, vol. 23, no. 11, pp. 20 652–20 663, 2022.

[11] M. A. M. Yussof, N. H. Amer, Z. A. Kadir, K. Hudha, M. S. Rahmat, and M. H. Harun, "Yaw stability control of single-trailer truck using steerable wheel at middle axle: hardware-in-the-loop simulation," *International Journal of Dynamics and Control*, vol. 10, no. 6, pp. 2072–2094, 2022.

[12] A. E. B. Ibrahim, "Self-tuning look-ahead distance of pure-pursuit path-following control for autonomous vehicles using an automated curve information extraction method," *International Journal of Intelligent Transportation Systems Research*, vol. 20, no. 3, pp. 709–719, 2022.

[13] A. AbdElmoniem, A. Osama, M. Abdelaziz, and S. A. Maged, "A path-tracking algorithm using predictive stanley lateral controller," *International Journal of Advanced Robotic Systems*, vol. 17, no. 6, p. 1729881420974852, 2020.

[14] S. Dixit, S. Fallah, U. Montanaro, M. Dianati, A. Stevens, F. Mccullough, and A. Mouzakitis, "Trajectory planning and tracking for autonomous overtaking: State-of-the-art and future prospects," *Annual Reviews in Control*, vol. 45, pp. 76–86, 2018.

[15] S. Dominguez, A. Ali, G. Garcia, and P. Martinet, "Comparison of lateral controllers for autonomous vehicle: Experimental results," in *2016 IEEE 19th International Conference on Intelligent Transportation Systems (ITSC)*. IEEE, 2016, pp. 1418–1423.

[16] S. Yu, M. Hirche, Y. Huang, H. Chen, and F. Allgöwer, "Model predictive control for autonomous ground vehicles: a review," *Autonomous Intelligent Systems*, vol. 1, pp. 1–17, 2021.

[17] L. Wang, *Model predictive control system design and implementation using MATLAB®*. Springer Science & Business Media, 2009.

[18] F. Yakub and Y. Mori, "Comparative study of autonomous path-following vehicle control via model predictive control and linear quadratic control," *Proceedings of the Institution of Mechanical Engineers, Part D: Journal of automobile engineering*, vol. 229, no. 12, pp. 1695–1714, 2015.

[19] D. Chu, H. Li, C. Zhao, and T. Zhou, "Trajectory tracking of autonomous vehicle based on model predictive control with pid feedback," *IEEE Transactions on Intelligent Transportation Systems*, vol. 24, no. 2, pp. 2239–2250, 2022.

[20] D. Q. Mayne and E. C. Kerrigan, "Tube-based robust nonlinear model predictive control1," *IFAC Proceedings Volumes*, vol. 40, no. 12, pp. 36–41, 2007.

[21] J. Löfberg, *Minimax approaches to robust model predictive control*. Linköping University Electronic Press, 2003, vol. 812.

[22] A. Mesbah, "Stochastic model predictive control: An overview and perspectives for future research," *IEEE Control Systems Magazine*, vol. 36, no. 6, pp. 30–44, 2016.

[23] D. Q. Mayne, "Model predictive control: Recent developments and future promise," *Automatica*, vol. 50, no. 12, pp. 2967–2986, 2014.

[24] R. Soloperto, J. Köhler, F. Allgöwer, and M. A. Müller, "Collision avoidance for uncertain nonlinear systems with moving obstacles using robust model predictive control," in *2019 18th European Control Conference (ECC)*. IEEE, 2019, pp. 811–817.

[25] D. Jeong, G. Ko, and S. B. Choi, "Estimation of sideslip angle and cornering stiffness of an articulated vehicle using a constrained lateral dynamics model," *Mechatronics*, vol. 85, p. 102810, 2022.

[26] M. El-Gindy and Z. El-Sayegh, *Road and Off-Road Vehicle Dynamics*. Springer Nature, 2023.

[27] Y. Hou and X. Xu, "High-speed lateral stability and trajectory tracking performance for a tractor-semitrailer with active trailer steering," *PloS one*, vol. 17, no. 11, p. e0277358, 2022.

[28] G. Bai, L. Liu, Y. Meng, W. Luo, Q. Gu, and B. Ma, "Path tracking of mining vehicles based on nonlinear model predictive control," *Applied Sciences*, vol. 9, no. 7, p. 1372, 2019.

[29] H. Yuan, D. Zhang, and T. Gordon, "Road vehicle rollover prevention torque vectoring via model predictive control," in *2017 36th Chinese Control Conference (CCC)*. IEEE, 2017, pp. 9401–9406.

[30] T. Xin, J. Xu, C. Gao, and Z. Sun, "Research on the speed thresholds of trucks in a sharp turn based on dynamic rollover risk levels," *PloS one*, vol. 16, no. 8, p. e0256301, 2021.

[31] I. B. Potts, D. W. Harwood, and K. R. Richard, "Relationship of lane width to safety on urban and suburban arterials," *Transportation research record*, vol. 2023, no. 1, pp. 63–82, 2007.

[32] J. B. Rawlings, D. Q. Mayne, and M. Diehl, *Model predictive control: theory, computation, and design*. Nob Hill Publishing Madison, WI, 2017, vol. 2.

[33] Z. Huang, P. Wang, L. Lu, and Z. Song, "An improved line-of-sight guidance law for path following of unmanned surface vehicle based on adaptive lookahead distance," in *International Conference on Mechanical Design and Simulation (MDS 2022)*, vol. 12261. SPIE, 2022, pp. 37–43.

[34] B. Stellato, G. Banjac, P. Goulart, A. Bemporad, and S. Boyd, "Osqp: An operator splitting solver for quadratic programs," *Mathematical Programming Computation*, vol. 12, no. 4, pp. 637–672, 2020.

Dasol Jeong received the B.S. degree in mechanical engineering from the Korea Advanced Institute of Science and Technology (KAIST), Daejeon, Korea, in 2017, the M.S. in mechanical engineering from KAIST, in 2019, and the Ph.D. degree in mechanical engineering from KAIST, in 2023. Since 2023, he has been the senior research engineer of the Hyundai Motor Company. His research interests include vehicle dynamics and control, intelligent tires, path planning, model predictive control, and control theory.

Seibum B. Choi (M'09) received the B.S. in mechanical engineering from Seoul National University, Seoul, Korea, the M.S. in mechanical engineering from KAIST, Deajeon, Korea, and the Ph.D. in control from the University of California, Berkeley, CA, USA, in 1993. From 1993 to 1997, he was involved in the development of automated vehicle control systems at the Institute of Transportation Studies, University of California. Through 2006, he was with TRW, Livonia, MI, USA, where he was involved in the development of advanced vehicle control systems. Since 2006, he has been faculty in the Mechanical Engineering Department, KAIST, Korea. His current research interests include fuel-saving technology, vehicle dynamics and control, and active safety systems. Prof. Choi is a Member of the American Society of Mechanical Engineers, the Society of Automotive Engineers, and the Korean Society of Automotive Engineers.